

## Proposed Superconducting Electride $\text{Li}_6\text{C}$ by $sp$ -Hybridized Cage States at Moderate Pressures

Zhao Liu,<sup>1</sup> Quan Zhuang,<sup>1,3</sup> Fubo Tian,<sup>1</sup> Defang Duan,<sup>1</sup> Hao Song,<sup>1</sup> Zihan Zhang,<sup>1</sup>  
Fangfei Li,<sup>1</sup> Hongdong Li,<sup>1</sup> Da Li<sup>⊕,1,\*</sup> and Tian Cui<sup>⊕,2,1,†</sup>

<sup>1</sup>State Key Laboratory of Superhard Materials, College of Physics, Jilin University, Changchun 130012, People's Republic of China

<sup>2</sup>School of Physical Science and Technology, Ningbo University, Ningbo 315211, People's Republic of China

<sup>3</sup>Inner Mongolia Key Laboratory of Carbon Nanomaterials, Nano Innovation Institute (NII), College of Chemistry and Materials Science, Inner Mongolia University for Nationalities, Tongliao 028000, People's Republic of China



(Received 16 November 2020; revised 19 July 2021; accepted 1 September 2021; published 8 October 2021)

The combination of electride state and superconductivity within the same compound, e.g.,  $[\text{Ca}_{24}\text{Al}_{28}\text{O}_6]^{4+}(4e^-)$ , opens up a new category of conventional superconductors. However, neither the underlying causations to explain superconducting behaviors nor effects of interstitial quasiatoms (ISQs) on superconductivity remain unclear. Here we have designed an efficient and resource-saving method to identify superconducting electrides only by chemical compositions and bonding characteristics. A representative superconducting electride  $\text{Li}_6\text{C}$  with a noteworthy  $T_c$  of 10 K below 1 Mbar among the known binary electrides has been revealed. Our first-principles studies unveil that the anomalous  $sp$ -hybridized cage-state ISQs, as a guest in  $\text{Li}_6\text{C}$ , exhibit unexpected ionic and covalent bonds, which act as a chemical precompression to lower dynamically stable pressure. More importantly, we uncover that, contrary to common expectations, the high  $T_c$  is attributed to the strong electron-phonon coupling derived from the synergy of interatomic coupling effect, phonon softening caused by Fermi surface nesting, and phonon-coupled bands, which are mainly dominated by host  $sp$ -hybridized electrons, rather than the ISQs. Our present results elucidate a new superconducting mechanism of electrides and shed light on the way for seeking a high- $T_c$  superconductor at lower pressures in cage-state electrides.

DOI: [10.1103/PhysRevLett.127.157002](https://doi.org/10.1103/PhysRevLett.127.157002)

Electrides stand for a class of exotic compounds where valence electrons detach from atoms and reside in the interstitial sites serving as anions without nuclei [1]. Topological electride states with multiple dimensions and abundant physicochemical properties triggered by pressure have attracted intense research interest [2]. Peculiarly, metallic electrides exhibit superconductivity that is quite different from that of well-known high-pressure superconductors, such as covalent magnesium diboride [3], elemental lithium [4,5], metallic hydrogen [6], hydrides  $\text{H}_3\text{S}$  [7],  $\text{LaH}_{10}$  [8], and carbonaceous sulfur hydride [9], opening up a new field of conventional superconductors. This has been observed for more complex metallic superconducting electrides, such as for  $[\text{Ca}_{24}\text{Al}_{28}\text{O}_6]^{4+}(4e^-)$  [(C12A7:  $e^-$ )] [10],  $\text{Mn}_5\text{Si}_3$ -type  $\text{Nb}_5\text{Ir}_3$  and  $\text{Zr}_5\text{Sb}_3$  system [11], and  $\text{Li}_6\text{P}$  with a noteworthy  $T_c$  of 39.3 K at superhigh pressures above 270 GPa [12]. Nevertheless, the studies of electride states with a relative high  $T_c$  at lower pressure are hampered [13], largely because the promotional [14] or suppression [15] effects of ISQs on the underlying superconducting mechanisms remain elusive. While several electrides have been revealed via a high-throughput material screening process [16], the developed process is highly inefficient due to its reliance on the terribly small number of known electrides in crystal

structure databases. Accordingly, it is highly desired to design an efficient, resource-saving, and simple calculation-aided criterion to identify fingerprints of electrides.

Pressure-induced dimensional changes of electride states may be a key factor related to the  $T_c$  values and required pressures. Upon pressure, in zero-dimensional (0D) electrides, ISQs keep “cage states” because they become trapped in interstitial cavities, and are assumed to induce narrow electronic band structures [17]. In one-dimensional (1D) electrides, ISQs are entrapped in channel cavities that form tubular building blocks [18]. In two-dimensional (2D) electrides, ISQs are similar to free electron gases, and are loosely restricted in interlayers, which lead to broad electronic band structures. Supposing that electride states have a large intrinsic coupling with phonons at the Fermi level ( $E_F$ ), this will be more than beneficial to superconductivity. Analyses have demonstrated that 2D electrides are favorable for increasing the possibility of metallization [19]. But unexpectedly, previous studies have demonstrated that increasing pressures generally induce dimensional reduction of ISQs from 2D, 1D to 0D electride states [20]. Moreover, the high activity of 2D electrides is also accompanied by the demerit of lower stability [21], and high pressure is needed to maintain dynamic stability. Strikingly, cage-state ISQs in a sodium host lattice can

shape what appear to be chemical bonds with adjacent host atoms [2]. For seeking electride superconductors stable at low pressures, subsequently, we speculate that the cage-state ISQs with chemical bonds [22] may effectively enhance the interactions between host-guest or host-host ions acting as chemical precompressions to lower dynamically stable pressure. Furthermore, strong chemical bonds in these particular host-guest configurations procreate bands extension and orbitals overlap, and increase the degree of metallization, which are helpful for supporting superconductivity.

In this Letter, we report a moderate pressure-induced superconducting electride  $\text{Li}_6\text{C}$  with a noteworthy  $T_c$ , obtained from our designed efficient screening method in conjunction with first-principles calculations. This method can significantly avoid the blindness of conventional high-throughput screening and consumption of computing resources. Importantly, our studies prove, contrary to common expectations, a new superconducting mechanism to elucidate superconducting behaviors of  $\text{Li}_6\text{C}$ , that is, the host  $sp$ -hybridized electrons dominating electron-phonon coupling  $\lambda$  and  $T_c$  rather than the ISQs. Intriguingly, the covalent bonding role played by  $sp$ -hybridized cage-state ISQs serves as an unexpected chemical precompression, resulting in a much lower predicted dynamically stable pressure of 40 GPa for  $\text{Li}_6\text{C}$  than that of  $\text{Li}_6\text{P}$  at 270 GPa. These findings offer a novel and key insight into the superconducting behaviors of electrides and provide a feasible demonstration for achieving relatively high- $T_c$  superconductors at lower pressure in cage-state electrides.

We screen potential superconducting electrides in low atomic number ( $Z$ ) carbides and nitrides model system based on the two facts. (i) Low- $Z$  elements are helpful for increasing the  $T_c$  owing to the propensity for the light masses of these elements to induce quite high phonon frequencies. (ii) Being conducive to forming electrides, the elements C and N with high electronegativity values of 2.55 and 3.04 can easily attract electrons from the low- $Z$  elements while allow some electrons to populate separately interstitial orbits [23]. For known binary Zintl-Klemm compounds with stoichiometric composition  $M_mX_x$  ( $M = \text{Al, Li, Be, B, Na, and Mg}$ ;  $X = \text{C and N}$ ) in Fig. 1, the valence electron concentration ( $C_{ve}$ ) of electronegativity atoms in Eq. (1) can prejudice bonding characteristics of sublattices (polycationic, polyanionic, or simple ionic structures) [24]. In Eq. (2),  $e(M)$  and  $e(X)$  represent the numbers of valence electrons for the respective electro-positive and electronegative elements;  $m$  and  $x$  corresponding to their number of atoms, respectively.  $E$  is lone electron pairs attached to atoms.  $b(MM)$  and  $b(XX)$  are the respective numbers of covalent bonds acting between  $M$  species and between  $X$  species, which are determined according to bond lengths or standard atomic radius.  $R$  represents the number of ISQs [Eq. (3)]. To be electrides,

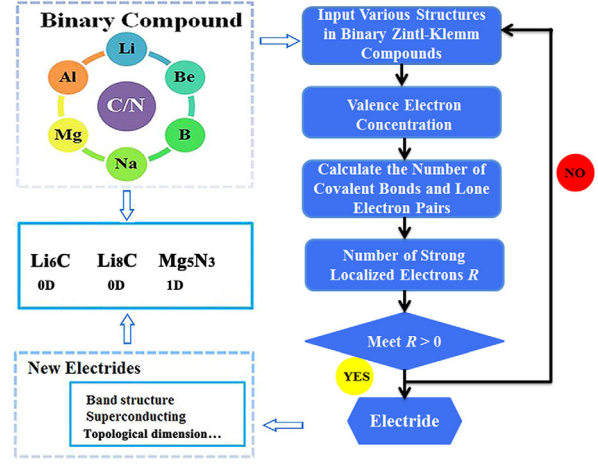


FIG. 1. Schematic illustrating the proposed calculation-aided methodology for identifying potential electrides.

the electron-rich condition,  $R > 0$ , is obtained. Then the electron localization function (ELF) [25] is calculated to identify topological dimensions. Application of the proposed method identified and confirmed three previously unreported electrides  $\text{Li}_6\text{C}$ ,  $\text{Li}_8\text{C}$ , and  $\text{Mg}_5\text{N}_3$  with a large  $R$  having 2, 4, and 1 formal charges per formula units (f.u.) (see [26]).

$$C_{ve}(X) = [m * e(M) + x * e(X)]/x, \quad (1)$$

$$m * [e(M) - b(MM) - E - R] + x * [e(X) + b(XX)] = 8x, \quad (2)$$

$$R = (x * [C_{ve}(X) - 8] + x * b(XX) - m * [b(MM) + E])/m. \quad (3)$$

Taking cage-state electride  $\text{Li}_6\text{C}$  as an illustration, in addition to the anti- $\text{CdCl}_2$ -I phase [39,40] disclosed by our method, we predict a new energy-preferred anti- $\text{CdCl}_2$ -II phase after a bidirectional structure search via the swarm intelligence-based methodology (CALYPSO) [41] and the evolutionary algorithm (USPEX) [42]. The enthalpy versus pressure curves indicate that the anti- $\text{CdCl}_2$ -type phases have the lowest formation enthalpies within 25–90 GPa. The zero-point-energy effects are too small to affect the sequence of phase transitions, and have accordingly been neglected. The crystalline  $\text{Li}_6\text{C}$  adopts a hexagonal conventional cell, and generally, this structure can be described by the cubic packing of Li and C atoms, where the body-centered position is occupied by C atom. An applied pressure converts the carbon occupation from the body-centered positions to the vertices of the primitive cell of the anti- $\text{CdCl}_2$ -II phase [Figs. 2(c) and 2(d)]. At 48 GPa, the volume variations evidence a second-order phase transition. The volume decreased almost linearly with increasing pressure by a factor of  $0.63 \text{ \AA}^3/\text{GPa}$  for the anti- $\text{CdCl}_2$ -I

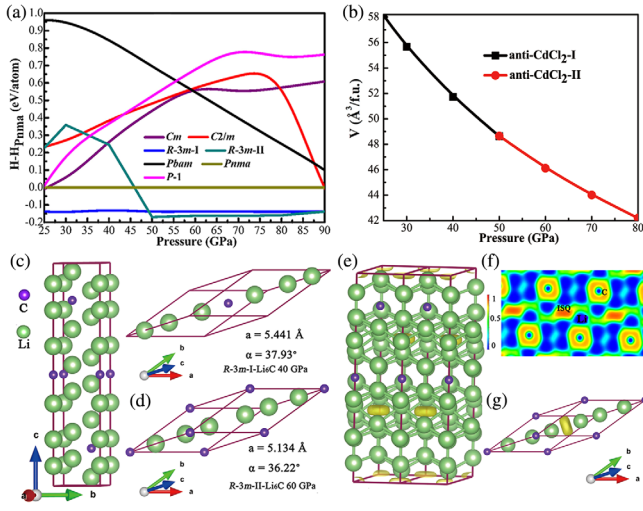


FIG. 2. Formation enthalpies and structural characteristics of  $\text{Li}_6\text{C}$ : (a) Formation enthalpies of predicted phases as a function of pressures. (b) Volume versus pressure for anti- $\text{CdCl}_2$ -I and II phases. (c) The anti- $\text{CdCl}_2$ -I phase at 40 GPa (d) anti- $\text{CdCl}_2$ -II phase at 60 GPa. (e) 3D isosurface (isosurface of 0.85) of ELF and (f) a 2D map of the (110) plane in anti- $\text{CdCl}_2$ -I phase at 40 GPa. (g) 3D isosurface of anti- $\text{CdCl}_2$ -II- $\text{Li}_6\text{C}$  at 60 GPa.

phase while  $0.22 \text{ \AA}^3/\text{GPa}$  for the anti- $\text{CdCl}_2$ -II phase in Fig. 2(b), implying ISQs respond more sensitive to compression in the anti- $\text{CdCl}_2$ -II phase. Molecular dynamic simulations demonstrate that anti- $\text{CdCl}_2$ -II phases possess superb thermal stability (see Supplemental Material Fig. S3 [26]). Figures 2(e)–2(g) confirm that ISQs with anomalous  $sp$ -hybridized (will be proved later) cage states are entrapped at intervals to balance the cationic charge showing ionic features. The Shannon ionic radius of the interstitial site ( $0.621 \text{ \AA}$ ) is comparable to the size of Li radius ( $0.760 \text{ \AA}$ ). Intriguingly, these  $sp$ -hybridized electronegative states act as bridges linking the charged carbons to form electron-conducting channels, which is the opposite function of isolated ISQs observed in transparent dense sodium [2,43].

The anti- $\text{CdCl}_2$ -type structures act out a metallic nature as revealed in Fig. 3(a) and Supplemental Material Fig. S5 [26]. At 40 GPa, the anti- $\text{CdCl}_2$ -I phase exhibiting strong host-guest bands coupling to dominate DOS near the  $E_F$  could be analogous to the  $C2/c$ - $\text{Li}_6\text{P}$  above 270 GPa. But  $\text{Li}_6\text{C}$  requires only 25 GPa to maintain dynamic structural stability with electride states. To elucidate the major role of ISQs in reducing the dynamically stable pressure, we analyzed the Li-Li interactions with and without intervening ISQs via integral crystal orbital Hamiltonian population (ICOHP) results [44] [see Fig. 3(c)]. Typical chemical bonds between nearest neighbor Li atoms without intervening ISQs are accompanied by negligible ICOHP values of  $-0.64$ ,  $-0.69$ , and  $-0.77 \text{ eV}$  at pressures of 40, 60, and 80 GPa, respectively. Conversely, the bonding energy between Li atoms with intervening ISQs becomes six to

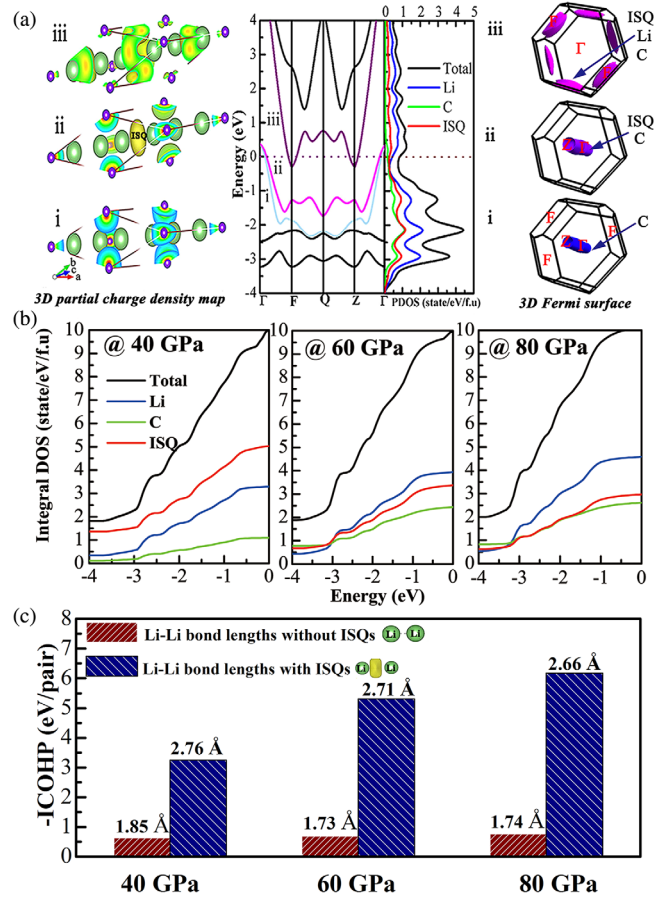


FIG. 3. Density of state and bonding characteristics of the anti- $\text{CdCl}_2$ -II phase at 60 GPa: (a) 3D partial charge density maps (isosurface of 0.015), projected density of states (PDOS), and Fermi surfaces for the bands labeled i, ii, and iii; (b) integral DOS values at  $E_F$  on a per f.u. basis; (c) calculated ICOHP values and Li-Li bond lengths with intervening ISQs and without intervening ISQs under different pressures.

ten times higher than those obtained without intervening ISQs, even though the Li-Li distance is much larger than the nearest neighbor. Cage-state ISQs play a role of covalent bonds to combine like-charge cations acting as a chemical precompression. For calibration, the energy of covalent bonds can be compared with C–C bond in diamond ( $-6.52 \text{ eV}$ ,  $P = 1 \text{ atm}$ ) [2]. The pressure-enhancing host-guest-host (lithium-ISQ-lithium) chemical bonding indicates that enthalpy turns lower, lattice becomes denser and volume gets smaller. A smaller volume hints a smaller  $PV$  term upon compression which, in turn, means a lower enthalpy.

The effects of chemical precompression on electronic properties, in turn, are reflected in band structures. The anti- $\text{CdCl}_2$ -II phase exhibits three strikingly broadening bands, marked as i, ii, iii crossing  $E_F$ , as depicted in Fig. 3(a). The corresponding projection of partial charge densities onto the constituent atoms is displayed in the left-hand panel. The DOS and 3D Fermi surface reflect the

hybridized states of Li-*s*, C-*p*, and ISQ orbitals. The ISQs are considered to be a characteristic of 2*p*-block element because band ii could be decomposed into C-*p* orbitals at the vertex and ISQ orbitals at the center. The similar topological features among ISQ, C-*p*, and Li-*s* orbitals constitute band iii, suggesting ISQs have characteristics of *s/p* orbitals. The above analyses indicate ISQs coupled with Li-*s* and C-*p* orbitals forming *sp*-hybridized states. Likewise, the highly dispersed paraboliclike band iii multiply crosses the  $E_F$ , suggesting strong interatomic coupling interactions and high group velocities of Li-C-*sp*-hybridized electrons (see Fig. S4 [26]).

For bands of anti-CdCl<sub>2</sub>-I phase in Fig. S5 [26], the “flat band–steep band” slopes around  $E_F$  resemble an advantageous condition for promoting the formation of Cooper pairs, which are critical for the phonon-mediated superconductivity and favor enhancement of electron-phonon interactions. Noteworthy, for the anti-CdCl<sub>2</sub>-II phase in Fig. 3(a), the steep conduction band iii shapes an “electron pocket” at the *F* and *Z* points, and this will lead to strong electron-phonon coupling (EPC) interactions, implying Li<sub>6</sub>C may be a high- $T_c$  superconductor [45].

As expected, the  $T_c$ 's of Li<sub>6</sub>C are estimated 4.2 ~ 10.0 K at 40 ~ 80 GPa, which are much higher than that of the first superconducting electride [Ca<sub>12</sub>Al<sub>14</sub>O<sub>32</sub>]<sup>2+</sup>·2*e*<sup>-</sup> with  $T_c$  ~ 1.79 K at 4.7 GPa [46]. To investigate the superconductivity and ferret out the role of cage-state ISQs played on Li<sub>6</sub>C, we calculate the lattice phonons in conjunction with EPC analyses, as depicted in Fig. 4(a), and disclose the  $T_c$  difference between (Li)<sub>6</sub><sup>+</sup>(C)<sup>4-</sup>·2*e*<sup>-</sup> and (Li)<sub>4</sub><sup>+</sup>(C)<sup>4-</sup> [39]. Both of them crystallize into anti-CdCl<sub>2</sub> phase at 60 GPa but are provided with different formal charges. Combining the analytical Eliashberg function  $\alpha^2F(\omega)$  and integrated EPC parameter  $\lambda$ , the  $\omega_{\log}$  is 437 K and  $\lambda$  reaches 0.52 in Li<sub>6</sub>C. Based on the calculated electron-phonon integral  $\lambda(\omega)$ , the EPC  $\lambda$  are mainly contributed by two parts. (i) A contribution of ~41.20% by the phonon modes above 10 THz. It shows a strong dependency of optical phonon frequencies on wave vector originated from the interatomic coupling effect, which would elevate the probability of satisfying the formation energy of Cooper pairs and be beneficial to strong EPC [47]. (ii) The contribution of ~58.80% from the low-frequency modes below 10 THz with distinct soft phonon modes [see Fig. 4(a) and Supplemental Material Fig. S6 [26]], which would play a significant role in enhancing the EPC  $\lambda$ . As for anti-CdCl<sub>2</sub> phase of Li<sub>4</sub>C, the weak EPC  $\lambda$  only stays 0.21 resulting in  $T_c$  approaching 1 K, as a contrasting counterpart, suggesting that the implanted lithium atoms coupling with derivative ISQs play a crucial role in enhancing the  $T_c$  of Li<sub>6</sub>C. That EPC divergences inspire us to split it, traced back to Hopfield expression  $\lambda = [N(E_F)\langle I^2 \rangle / M\omega^2]$  [48], into a purely electronic property originated from DOS and a parameter  $\eta = (I^2 / M\omega^2)$  [15] related to the lattice effects. The  $N(E_F)$  is for a single spin per atom, and  $\langle I^2 \rangle$  delegates

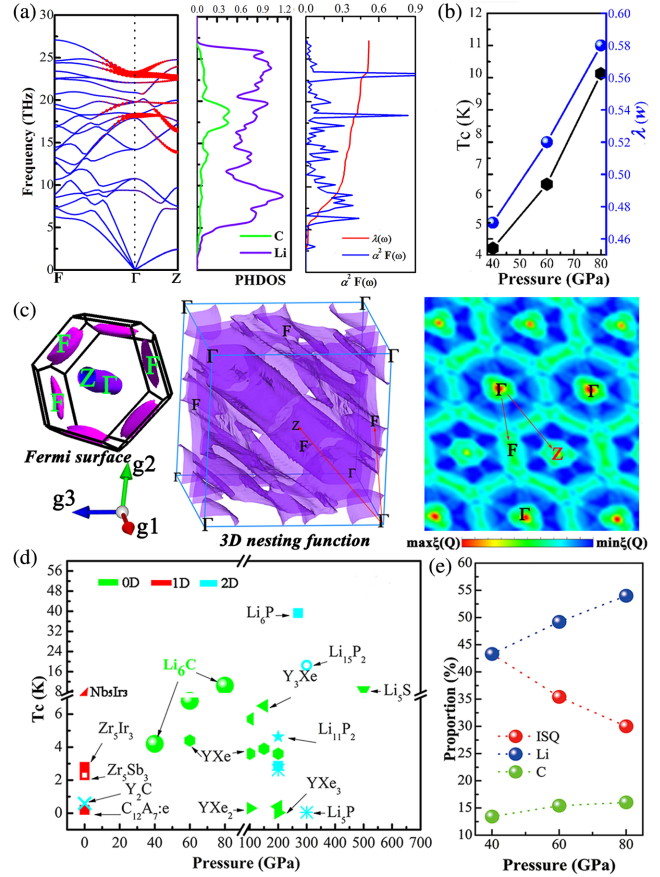


FIG. 4. (a) Phonon dispersion, projected phonon DOS, Eliashberg spectral function  $\alpha^2F(\omega)$  with integrated EPC parameter  $\lambda(\omega)$  at 60 GPa. Red solid circles represent the phonon linewidth with a radius proportional to the strength. (b) Values of  $\lambda$  and  $T_c$  as a function of pressures. (c) Fermi surface and 3D and 2D (0.8 0.3–0.3) plane nesting function  $\xi(Q)$  calculated with  $60 \times 60 \times 60$  mesh in a primitive cell of reciprocal space. (d)  $T_c$ 's versus pressure for representative superconducting electrides [11,49–51]. (e) Contributions of different atoms to the total DOS at the  $E_F$ .

the average over the Fermi surface of the electron-phonon matrix element squared.

In terms of electronic effect, we note that total numbers of ISQs decrease with elevated pressures in Fig. 3(b), and interstitial orbitals stretch to deep states ( $<E_F$ ) in Fig. S7 [26]. ISQs become increasingly confined to empty cavities without itinerant, possessing little coupling with lattice vibrations. However, analyses show the  $T_c$  evolution, in Fig. 4(b), increased with a pressure coefficient of 0.145 K/GPa. Next, we quantified the occupied states of electrons at  $E_F$  and found that the proportion of ISQs decreased greatly with pressurization in Fig. 4(e), leading to an increased proportion of free electrons derived from Li/C although there is a slight decrease in  $N(E_F)$  (see Table S2 [26]). The variational trends of  $\lambda$  and  $T_c$  are inversely proportional to the proportion in  $N(E_F)$  and total numbers of ISQs, but are directly proportional to the

proportion in  $N(E_F)$  and total numbers of  $sp$ -hybridized states of Li/C. This indicates that the increasing EPC is mainly attributed to number-increased  $sp$ -hybridized host electrons. Given that more Li/C- $sp$ -hybridized bands multiply cross the Fermi surface in the anti-CdCl<sub>2</sub>-II phase, more modes with various wave vectors will be generated and scattered into Cooper pairs. Furthermore, the  $sp$ -hybridized states become stronger with pressurization due to the enhanced bonding bands switching to deep level (see Figs. S7, S8 [26]). These  $sp$ -hybridized states are expected to have higher freedoms of orbital multiplicity and more easily form stable Cooper pairs [52] than Li- $s$ -electrons, which is similar to the mechanism of superconductivity induced by pressure, from  $s$  states to non- $s$  states, in alkali metals [53], elaborated by Hosono *et al.* [54]. In conjunction with the band analysis, one factors of anomalous  $T_c$  enlargement with decreasing  $N(E_F)$  is attributed to the strong EPC that mainly derived from the phonon-coupled bands dominated by host  $sp$ -hybridized states in view of DOS.

In terms of lattice effect, in Table S2 [26], we note the  $\eta$  (8.12, eV/atom) of the anti-CdCl<sub>2</sub>-II phase at 80 GPa is 2.22 times as much as  $\eta$  (3.66) of anti-CdCl<sub>2</sub>-I phase at 40 GPa, which agree well with the evolution in  $T_c$  (increased by a multiplicative factor of 2.38). In fact, the prominent phonons softening mainly occurring below 10 THz, in Fig. 4(a), along  $\Gamma \rightarrow Z$  and  $\Gamma \rightarrow F$  symmetric paths, played a significant role in enhancing EPC [45,55,56]. Because such  $sp$ -hybridized states close to  $E_F$  could effectively shield the lattice vibrations involving Li atoms [48], thereby it leads to promotions of  $\lambda$ . The scale of such phonon softening remains stiff and sustainable with pressurization. To uncover the secret of phonon softening, we plot the Fermi surface nesting based on the formula  $\xi(Q)$ :

$$\xi(Q) = \frac{1}{N} \sum_{k,i,j} \delta(\epsilon_{k,i} - \epsilon_F) \times \delta(\epsilon_{k+Q,j} - \epsilon_F).$$

Not coincidentally, we can clearly find that the routes of phonon softening below 10 THz correspond to the nesting directions along  $Q_\Gamma$  to  $Q_z$  and to  $Q_F$  in Fig. 4(c). This result perfectly explained soft phonon modes caused by Fermi surface nesting. Combining with band structures analyses in Fig. 3(a), this nesting is associated with host electrons, one pocket (electronlike) Fermi surface tracing back to band iii and the other tubular Fermi surface (holelike) from band i and band ii. A pocket and two tubular Fermi surfaces are nested with each other corresponding to the obvious nesting vectors along the  $\Gamma \rightarrow F$  direction. Contrasting with the well-separated number-increased host electrons and number-declined ISQs with pressurization in Fig. 3(b), host  $sp$ -hybridized states are a dominated contributor to EPC.

The known typical superconducting electrides with high  $T_c$  have been reviewed in Fig. 4(d). Significant progresses have been made in improving the  $T_c$ 's by effectively tailoring

electride dimensions via the application of high pressure. The calculated  $T_c$  of Li<sub>6</sub>C at 80 GPa is greater than that of most electrides at high pressures. In sharp contrast to 2D electride states, the guest cage-state ISQs participating in chemical bonds and serving as a chemical precompression to lower dynamically stable pressure are feasible.

In summary, we report an effective computer-assisted methodology, combining  $C_{ve}$  and generalized octet rule, to identify pressure-induced Li<sub>6</sub>C, Li<sub>8</sub>C, and Mg<sub>5</sub>N<sub>3</sub> electrides in low- $Z$  carbides and nitrides. Our first-principles analyses indicate that the Li<sub>6</sub>C is a potential superconductor,  $T_c$ 's of 4.2 ~ 10.0 K from 40 to 80 GPa. Upon compression, we find the strong EPC mainly derived from the synergy of interatomic coupling effect, phonon softening and phonon-coupled bands dominated by number-increased host  $sp$ -hybridized electrons, which is a new mechanism supplemented to the guest ISQs dominated superconductivity. The unexpected  $sp$ -hybridized cage-state ISQs serving as a chemical precompression can lower dynamically stable pressure, which explains the moderate-pressure stabilization. Our current report provides powerful insights and guidance for seeking high- $T_c$  superconductors at moderate pressure in cage-state electrides.

This work was supported by the National Key R&D Program of China (No. 2018YFA0703404, No. 2017YFA0403704, No. 2016YFB0201204), National Natural Science Foundation of China (No. 91745203, No. 11474127, No. 11404134, No. 11574109). Program for Changjiang Scholars and Innovative Research Team in University (No. IRT\_15R23). Parts of calculations were performed in the High Performance Computing Center (HPCC) of Jilin University.

\*Corresponding author.  
dali@jlu.edu.cn

†Corresponding author.  
cuitian@jlu.edu.cn

- [1] M. S. Miao, R. Hoffmann, J. Botana, I. I. Naumov, and R. J. Hemley, *Angew. Chem. Int. Ed.* **56**, 972 (2017).
- [2] M. S. Miao and R. Hoffmann, *J. Am. Chem. Soc.* **137**, 3631 (2015).
- [3] J. Nagamatsu, N. Nakagawa, T. Muranaka, Y. Zenitani, and J. Akimitsu, *Nature (London)* **410**, 63 (2001).
- [4] T. Bazhurov, J. Noffsinger, and M. L. Cohen, *Phys. Rev. B* **82**, 184509 (2010).
- [5] K. Shimizu, H. Ishikawa, D. Takao, T. Yagi, and K. Amaya, *Nature (London)* **419**, 597 (2002).
- [6] R. P. Dias and I. F. Silvera, *Science* **355**, 715 (2017).
- [7] D. Duan, Y. Liu, F. Tian, D. Li, X. Huang, Z. Zhao, H. Yu, B. Liu, W. Tian, and T. Cui, *Sci. Rep.* **4**, 6968 (2015).
- [8] F. Peng, Y. Sun, C. J. Pickard, R. J. Needs, Q. Wu, and Y. Ma, *Phys. Rev. Lett.* **119**, 107001 (2017).
- [9] E. Snider, N. Dasenbrock-Gammon, R. McBride, M. Debessai, H. Vindana, K. Vencatasamy, K. V. Lawler, A. Salamat, and R. P. Dias, *Nature (London)* **586**, 373 (2020).

- [10] Y. Kohama, S. W. Kim, T. Tojo, H. Kawaji, T. Atake, S. Matsuishi, and H. Hosono, *Phys. Rev. B* **77**, 092505 (2008).
- [11] B. Lv, X. Y. Zhu, B. Lorenz, F. Y. Wei, Y. Y. Xue, Z. P. Yin, G. Kotliar, and C. W. Chu, *Phys. Rev. B* **88**, 134520 (2013).
- [12] Z. Zhao, S. Zhang, T. Yu, H. Xu, A. Bergara, and G. Yang, *Phys. Rev. Lett.* **122**, 097002 (2019).
- [13] L. A. Burton, F. Ricci, W. Chen, G. M. Rignanesi, and G. Hautier, *Chem. Mater.* **30**, 7521 (2018).
- [14] X. Zhang and G. Yang, *J. Phys. Chem. Lett.* **11**, 3841 (2020).
- [15] C. Kokail, C. Heil, and L. Boeri, *Phys. Rev. B* **94**, 060502 (R) (2016).
- [16] J. Zhou, L. Shen, M. Yang, H. X. Cheng, W. L. Kong, and Y. P. Feng, *Chem. Mater.* **31**, 1860 (2019).
- [17] Y. Tsuji, P. Dasari, S. F. Elatresh, R. Hoffmann, and N. W. Ashcroft, *J. Am. Chem. Soc.* **138**, 14108 (2016).
- [18] Y. Zhang, Z. Xiao, T. Kamiya, and H. Hosono, *J. Phys. Chem. Lett.* **6**, 4966 (2015).
- [19] K. Lee, S. W. Kim, Y. Toda, S. Matsuishi, and H. Hosono, *Nature (London)* **494**, 336 (2013).
- [20] H. Tang *et al.*, *Adv. Sci.* **5**, 1800666 (2018).
- [21] J. J. Wang, K. Hanzawa, H. Hiramatsu, J. Kim, N. Umezawa, K. Iwanaka, T. Tada, and H. Hosono, *J. Am. Chem. Soc.* **139**, 15668 (2017).
- [22] S. Matsuishi, Y. Toda, M. Miyakawa, K. Hayashi, T. Kamiya, M. Hirano, I. Tanaka, and H. Hosono, *Science* **301**, 626 (2003).
- [23] M. S. Miao and R. Hoffmann, *Acc. Chem. Res.* **47**, 1311 (2014).
- [24] U. Müller, *Inorganic Structural Chemistry*, 2nd ed. (John Wiley & Sons, Ltd, Wiley Online Library, 2006).
- [25] J. E. Lennard-Jones, *J. Chem. Phys.* **20**, 1024 (1952).
- [26] See Supplemental Material at <http://link.aps.org/supplemental/10.1103/PhysRevLett.127.157002> for detailed description of calculation methods, superconducting calculations, demonstration of the chosen of energy cutoff value, extended research on ternary electrides, the unit-cell parameters and atomic positions, electronic band structures and projected density of states of anti-CdCl<sub>2</sub>-I phase, 3D ELF of Li<sub>8</sub>C and Mg<sub>3</sub>N<sub>3</sub>, radial distribution function  $g(r)$  of anti-CdCl<sub>2</sub>-II at temperatures of 500 and 1000 K, phonon dispersion curves. Supplemental Material includes Refs. [27–38].
- [27] A. R. Oganov, C. W. Glass, and S. Ono, *Earth Planet. Sci. Lett.* **241**, 95 (2006).
- [28] A. Vanderlei dos Santos, G. Padhila, and M. Monçalves, *Solid State Sci.* **14**, 269 (2012).
- [29] P. E. Blöchl, *Phys. Rev. B* **50**, 17953 (1994).
- [30] J. Klimeš, D. R. Bowler, and A. Michaelides, *Phys. Rev. B* **83**, 195131 (2011).
- [31] E. R. Hernandez, *J. Chem. Phys.* **115**, 10282 (2001).
- [32] P. Giannozzi *et al.*, *J. Phys. Condens. Matter* **21**, 395502 (2009).
- [33] A. Togo, F. Oba, and I. Tanaka, *Phys. Rev. B* **78**, 134106 (2008).
- [34] S. Maintz, V. L. Deringer, A. L. Tchougreff, and R. Dronskowski, *J. Comput. Chem.* **34**, 2557 (2013).
- [35] R. D. Shannon, *Acta. Cryst.* **32**, 751 (1976).
- [36] P. B. Allen and R. C. Dynes, *Phys. Rev. B* **12**, 905 (1975).
- [37] Y. Zhang, W. Wu, Y. Wang, S. A. Yang, and Y. Ma, *J. Am. Chem. Soc.* **139**, 13798 (2017).
- [38] H. Tang *et al.*, *Adv. Sci.* **5**, 1800666 (2018).
- [39] X. Jin *et al.*, *Proc. Natl. Acad. Sci. U.S.A.* **113**, 2366 (2016).
- [40] Y. Z. Lin, T. A. Strobel, and R. E. Cohen, *Phys. Rev. B* **92**, 214106 (2015).
- [41] Y. C. Wang, J. Lv, L. Zhu, and Y. M. Ma, *Phys. Rev. B* **82**, 094116 (2010).
- [42] A. R. Oganov and C. W. Glass, *J. Chem. Phys.* **124**, 244704 (2006).
- [43] Y. Ma, M. Eremets, A. R. Oganov, Y. Xie, I. Trojan, S. Medvedev, A. O. Lyakhov, M. Valle, and V. Prakapenka, *Nature (London)* **458**, 182 (2009).
- [44] R. Dronskowski and P. E. Blochl, *J. Phys. Chem. A* **97**, 8617 (1993).
- [45] Y. B. Ma, D. Duan, Z. Shao, H. Yu, H. Liu, F. Tian, X. Huang, D. Li, B. Liu, and T. Cui, *Phys. Rev. B* **96**, 144518 (2017).
- [46] S. Tanaka, T. Kato, A. Miyake, T. Kagayama, K. Shimizu, S. W. Kim, S. Matsuishi, and H. Hosono, *J. Korean Phys. Soc.* **63**, 477 (2013).
- [47] Q. Zhuang, X. L. Jin, T. Cui, D. Zhang, Y. Li, X. Li, K. Bao, and B. B. Liu, *Phys. Rev. B* **98**, 024514 (2018).
- [48] N. I. Kulikov, *J. Phys. F* **8**, L137 (1978).
- [49] Y. Q. Zhang, B. S. Wang, Z. W. Xiao, Y. F. Lu, T. Kamiya, Y. Uwatoko, H. Kageyama, and H. Hosono, *npj Quantum Mater.* **2**, 45 (2017).
- [50] S. Dilmi, S. Saib, and N. Bouarissa, *Curr. Appl. Phys.* **18**, 1338 (2018).
- [51] D. W. Zhou, D. Szczesniak, J. H. Yu, C. Y. Pu, and X. Tang, *J. Phys. Chem. C* **123**, 9323 (2019).
- [52] C. Wang, S. Yi, and J. H. Cho, *Phys. Rev. B* **101**, 104506 (2020).
- [53] N. E. Christensen and D. L. Novikov, *Phys. Rev. Lett.* **86**, 1861 (2001).
- [54] H. Hosono, S. W. Kim, S. Matsuishi, S. Tanaka, A. Miyake, T. Kagayama, and K. Shimizu, *Phil. Trans. R. Soc. A* **373**, 20140450 (2015).
- [55] J. S. Tse, Y. Yao, and K. Tanaka, *Phys. Rev. Lett.* **98**, 117004 (2007).
- [56] H. Wang, J. S. Tse, K. Tanaka, T. Tanaka, and Y. Ma, *Proc. Natl. Acad. Sci. U.S.A.* **109**, 6463 (2012).